Ultrasonics Sonochemistry 71 (2021) 105374

Contents lists available at ScienceDirect

Ultrasonics Sonochemistry

journal homepage: www.elsevier.com/locate/ultson

Preparation of NiO decorated CNT/ZnO core-shell hybrid nanocomposites with the aid of ultrasonication for enhancing the performance of hybrid supercapacitors

Nagabandi Jayababu, Seungju Jo, Youngsu Kim, Daewon Kim *

Department of Electronic Engineering, Institute for Wearable Convergence Electronics, Kyung Hee University, 1732 Deogyeong-daero, Giheung-gu, Yongin 17104, Republic of Korea

ARTICLE INFO

Keywords:
Ultrasonication
Hybrid supercapacitor
NiO decoration
Carbon nanotubes
ZnO
Core-shell nanostructures

ABSTRACT

Supercapacitor (SC) electrodes fabricated with the combination of carbon nanotubes (CNTs) and metal oxides are showing remarkable advancements in the electrochemical properties. Herein, NiO decorated CNT/ZnO core-shell hybrid nanocomposites (CNT/ZnO/NiO HNCs) are facilely synthesized by a two-step solution-based technique for the utilization in hybrid supercapacitors. Benefitting from the synergistic advantages of three materials, the CNT/ZnO/NiO HNCs based electrode has evinced superior areal capacity of ~67 μAh cm^{-2} at a current density of 3 mA cm^{-2} with an exceptional cycling stability of 112% even after 3000 cycles of continuous operation. Highly conductive CNTs and electrochemically active ZnO contribute to the performance enhancement. Moreover, the decoration of NiO on the surface of CNT/ZnO core-shell increases the electro active sites and stimulates the faster redox reactions which play a vital role in augmenting the electrochemical properties. Making the use of high areal capacity and ultra-long stability, a hybrid supercapacitor (HSC) was assembled with CNT/ZnO/NiO HNCs coated nickel foam (CNT/ZnO/NiO HNCs/NF) as positive electrode and CNTs coated NF as negative electrode. The fabricated HSC delivered an areal capacitance of 287 mF cm^{-2} with high areal energy density (67 μWh cm^{-2}) and power density (16.25 mW cm^{-2}). The combination of battery type CNT/ZnO/NiO HNCs/NF and EDLC type CNT/NF helped in holding the capacity for a long period of time. Thus, the systematic assembly of CNTs and ZnO along with the NiO decoration enlarges the application window with its high rate electrochemical properties.

1. Introduction

Unimaginable growth of global population is demanding the high amount of energy, and tending to destroy the environment with the pollutants releasing from the conventional energy sources (coal, gas, oil, etc.) [1–3]. These ever-increasing energy-environmental problems have been stimulating the exploration towards alternative clean energy resources such as solar, wind, ocean, and bio energies [4–7]. Most of the renewable and environmentally benign energy sources are sporadic in nature, and need an energy storage device arrangement besides it [1]. Thus, the demand is increased for the best performing energy storage technology/device to buffer the intermittent nature of the sustainable energy sources.

Two major technologies which occupied the energy storage industry are lithium-ion batteries (LIBs) and supercapacitors (SCs) [8]. Each technology is possessing its own advantages along with disadvantages. With peculiar features such as sharp charge/discharge rates, high power densities, improved cycling stabilities, and simple and safe operations, SCs are drawing utmost attention in the field of energy storage [9–11]. Specifically, hybrid supercapacitors (HSCs), which are derived from the blend of electric double layer capacitor (EDLC) electrode and battery type electrode [12,13]. This HSCs entrust high energy density originated from rich redox chemistry of battery-type materials, and power density resulted from EDLC materials [12]. Moreover, the widening of potential window is also evident in this class of SCs due to the existence of two different electrode materials which enhances the energy density in line with the equation $E = ½ CV^2$ [8].

Recent reports on novel materials-based HSCs have been proclaimed enhanced performances than other supercapacitors benefiting from the advantages of two mechanisms [14–18]. As the performance of a SC is

* Corresponding authors.
E-mail address: daewon@khu.ac.kr (D. Kim).

https://doi.org/10.1016/j.ultsonch.2020.105374
Received 15 September 2020; Received in revised form 13 October 2020; Accepted 18 October 2020
Available online 22 October 2020

dependent on materials and their combination, the exploration of novel materials and combinations for next generation HSCs is a current scientific challenge in the field of energy storage. CNTs as a supercapacitor electrode are gaining the wide spread of attention owing to their unique properties, such as high surface area, high electrical conductivity, and excellent stability [19]. ZnO is a ubiquitous component in the battery type SCs with its numerous advantages like, high chemical stability, high energy density of 650 A g^{-1}, abundancy, good electrochemical activity, low cost, eco-benign nature, and ease of fabrication [20–22]. Utilizing the advantages of both the materials, improvement in the performance of the SC can be achieved by the combination of CNTs and ZnO with different morphologies. Recently, Ranjithkumar et al. fabricated ZnO nanorod embedded CNT (ZnO/CNT) by a chemical refluxing method and showed its superior electrochemical performance than individual ZnO or CNTs. ZnO/CNT electrode has shown a specific capacitance of 189 F g^{-1}, which is nearly 1.5 times of CNT electrode and 3 times of ZnO electrode [23]. In another study, Wei Wang et al. reported the enhanced electrochemical performance of ZnO/CNT electrodes prepared by a suction filtration method. The study revealed that the increase in the contents of CNTs and ZnO resulted in the enhanced electrochemical performance maximum areal capacitance at a scan rate of 50 mV s^{-1} is 14.6 mF cm^{-2} until the optimization point and then decreased [24]. Few other studies also proved that the fabrication of CNT and ZnO based composite electrodes gives the improved performance [25–27]. Surprisingly, a recent study related to CNTs uncovered the dramatical improvement in the performance of the composite electrode when it is combined with mixed metal oxides [28]. Thus, it is anticipated that the addition of second metal oxide can tremendously enhance the charge storage capacity of the CNT/ZnO composite. Moreover, a systematic assembly of metal oxides and CNTs is needed to achieve higher performances with longer lifetimes by facilitating the high surface area, and electrochemical active plats. Nickel oxide (NiO) is also a widely studied material as supercapacitor electrode due to its high theoretical capacitance (2584 F g^{-1}), environmental friendliness, low cost, facile synthesis, and good chemical stability [1,29,30]. Efficient decoration of NiO on the surface of CNT/ZnO core-shell nanostructures enhances the electrochemical performance by improving the active surface area, facilitating the effective diffusion of electrolyte, and contributing itself as an electro active material.

By considering the aforementioned facts, we have successfully fabricated the NiO decorated CNT/ZnO core-shell hybrid nanocomposites (CNT/ZnO/NiO HNCs) using facile solution-based method with the aid of ultrasonication for the enhancement of electrochemical performance of the HSC. Prior to the core-shell synthesis process, CNTs were refluxed for better dispersibility using ultrasonication. Refluxed CNTs were dispersed in Zn acetate solution to develop the ZnO shell on their surface. As obtained CNT/ZnO core-shell nanostructures were decorated by NiO with the aid of ultrasonication to achieve novel hybrid nanocomposites. Due to the collective advantages of the materials in the composite, CNT/ZnO/NiO HNCs/NF electrode has delivered high areal capacity than all other electrodes along with the excellent long-term cycling stability (over 3000 cycles). Finally, the assembled HSC by utilizing the CNT/ZnO/NiO hybrid nanocomposite as positive electrode and CNTs as negative electrode has demonstrated good electrochemical properties. Here, the novel core-shell structure of CNTs and ZnO improved the electro-active sites. The decoration of NiO on the CNT/ZnO core-shell surface further enhanced the active surface area of the electrode. Thus, the unique NiO decorated CNT/ZnO core-shell structure ultimately improved the diffusion rate of electrolyte ions into the electrode and thereby electrochemical performance.

2. Experimental

2.1. Materials

All the materials used in this experiment are reagent grade, and used as received without any further purification. CNTs, zinc acetate dihydrate ($Zn(CH_3CO_2)_2{\cdot}2H_2O$), nickel chloride hexahydrate ($NiCl_2{\cdot}6H_2O$), sodium hydroxide (NaOH), potassium hydroxide (KOH), and nitric acid (HNO_3) were supplied by Sigma Aldrich Co., Republic of Korea. Nickel foam (NF) and super P carbon were obtained from MTI Korea, Republic of Korea. Deionized (DI) water of 18.3 MΩ cm resistivity is produced within the laboratory using Milli-Q water filter system and utilized for the experiment.

2.2. Ultrasonication assisted functionalization of CNTs and preparation of CNT/ZnO, CNT/NiO core-shell nanostructures (CSNSs)

Prior to the core-shell synthesis process, the dispersity of CNTs was improved by chemical refluxing process with the aid of ultrasonication. 300 mg of CNTs was refluxed in 50 mL of 6 M concentrated HNO_3 solution for 4 h at 80 ℃, followed by washing with DI water, and drying overnight at 60 ℃.

Synthesis of CNT/ZnO CSNSs was facilely done by a solution-based method. In a typical synthesis process, 100 mg of functionalized CNTs was dispersed in 50 mL of DI water *via* ultrasonication for 30 min. Meanwhile, 10 mM of $Zn(CH_3CO_2)_2{\cdot}2H_2O$ solution was prepared by dissolving 110 mg of $Zn(CH_3CO_2)_2{\cdot}2H_2O$ in 50 mL of DI water. Then the CNTs dispersion was added to the Zn solution under magnetic stirring for 4 h at 80 ℃ by adding NaOH solution drop wise and soaked the mixture for a period of 6 h. After cooling down to room temperature, the precipitate was collected and washed with DI water and ethanol several times, followed by drying at 300 ℃ for 2 h to obtain CNT/ZnO CSNSs. Synthesis of CNT/NiO CSNSs was also performed in a similar manner by adding dispersed CNTs in 50 mL of 10 mM $NiCl_2{\cdot}6H_2O$ solution and proceeded until drying at 300 ℃ for 2 h.

2.3. Synthesis of CNT/ZnO/NiO HNCs with the aid of ultrasonication

To prepare CNT/ZnO/NiO HNCs, first 100 mg of CNT/ZnO CSNSs were dispersed in 50 mL of DI water using ultrasonication for 30 min and mixed with 50 mL of 5 mM $NiCl_2{\cdot}6H_2O$ solution. The mixture was stirred for 1 h at a temperature of 80 ℃ by adding NaOH drop wise. The well mixed precipitate was collected and washed with DI water several times. Ultimately, the CNT/ZnO/NiO HNCs were obtained after drying the precipitate at 300 ℃ for 2 h. Several other materials like, pure ZnO nanorods (NRs) and NiO nanosheets (NSs), and ZnO/NiO core-shell nanostructures (CSNSs) were also prepared for the comparison studies. Detailed description on their fabrication is given in electronic supplementary information (ESI, Fig S1).

2.4. Characterization

Field emission scanning electron microscope (FESEM, Carl Zeiss, LEO SUPRA 55) equipped with an energy dispersive X-ray spectroscopy (EDS) was employed to investigate the surface morphology and elemental composition of the synthesized materials. Transmission electron microscope (HR TEM, JEM 2100F, OXSFORD instruments) equipped with EDS was utilized for the examination of internal microstructure of the samples. The information related to crystalline nature and phase of the materials was obtained from X-ray diffraction (XRD, Cu Kα radiation, M18XHF-SRA, MAC Science) analysis. The surface elemental composition and oxidation states of the samples were analyzed by using X-ray photoelectron spectroscopy (XPS, Thermo Electron MultiLab2000).

2.5. Electrochemical measurements

All the electrodes were prepared by a simple slurry coating method using the nickel foam (NF) as a current collector. Cleaning of the NF was performed very carefully to remove the oxidative layer on the surface by sonicating it in HCl (37 wt%), water, and ethanol for 5 min at each step,

followed by drying. In order to prepare electrodes, the active material (ZnO NRs, NiO NSs, ZnO/NiO CSNSs, CNT/ZnO and CNT/NiO CSNSs, and CNT/ZnO/NiO HNCs), super P carbon, and PTFE binder were taken in a weight ratio of 80:10:10 and ground in an agate mortar by adding few drops of N-methyl-2-Pyrrolidone (NMP) until the formation of uniform slurry. This slurry was uniformly coated on professionally cleaned NF in an active area of 1 × 1 cm^2 and dried at 80 ℃ for 4 h followed by pressing with ~5 MPa pressure to obtain better attachment between the material and NF.

The electrochemical properties of the electrodes were investigated by using an IviumStat electrochemical instrument (IVIUM Technologies) with the help of cyclic voltammetry (CV), galvanostatic charge/discharge (GCD), and electrochemical impedance spectroscopy (EIS) in three electrode system at room temperature (Fig. S4). Synthesized materials coated NF was acted as working electrode, Pt wire was used as counter electrode, and Ag/AgCl was taken as reference electrode. The applicability of the best performing material (CNT/ZnO/NiO HNCs/NF) for practical applications was tested by fabricating supercapacitor device using it as positive electrode, CNTs coated NF (CNTs/NF) as negative electrode, 1 M KOH as electrolyte, and cellulose membrane as separator. The fabrication of negative electrode was also done in a similar manner as described above by coating CNTs slurry on NF. The following equations were used to obtain areal capacity, areal capacitance, energy density, and power densities [31].

$$Q = \frac{I \times \Delta t}{a} \tag{1}$$

$$C_a = \frac{I \times \Delta t}{a \times \Delta V} \tag{2}$$

$$E_d = \frac{C_a \times \Delta V^2}{2} \tag{3}$$

$$P_d = \frac{E_d}{\Delta t} \tag{4}$$

where, Q, C_a, E_d, and P_d are areal capacity (Ah cm^{-2}), areal capacitance (F cm^{-2}), areal energy density (Wh cm^{-2}), and areal power density (W cm^{-2}), respectively. I, a, Δt, and ΔV are current density (mA cm^{-2}), area (cm^2), discharging time (s), and potential window (V), respectively.

3. Results and discussion

3.1. Structural and morphological analysis

Fig. 1 schematically elucidates the NiO decorated CNT/ZnO core-shell nanostructures developed by a facile two step solution-based technique. Fig. 1a is the schematical representation of the functionalized CNTs. In first step, stirring followed by soaking of CNTs dispersion in Zn acetate dihydrate solution was conducted to coat ZnO shell on CNTs surface. During this process, the Zn precursor was uniformly developed on CNTs and strongly adhered to their surface. Drying at 300 °C induced the growth of the ZnO from the Zn precursor with perfect phase onto the surface of CNTs (Fig. 1b). During the second step, a mild stirring and heating helped to decorate NiO on CNT/ZnO core-shell nanostructures after immersing them in nickel precursor solution (Fig. 1c). Prior to this second step, the CNT/ZnO CSNS were well dispersed in DI water *via* ultrasonication for homogenous distribution of NiO nanoparticles on the core-shell surface. The main role of the ultrasonication in this experiment is to separate the agglomerated CNTs in order to develop the ZnO shell on their entire surface. After the ultrasonication process for 4 h, the surface of the CNTs is completely available to coat ZnO shell. Similarly, CNT/ZnO core-shell nanostructures were also subjected to ultrasonication for the proper separation of the agglomerated nanostructures before decorating with NiO. Due to its high chemical stability, good electrical conductivity, and large porosity, NF was selected as a current collector for the electrodes and coated the prepared materials on it. This highly porous conductive substrate collects the electrons from the electroactive materials and transport them to an external circuit rapidly [8].

Surface morphology of the CNTs, CNT/ZnO, and CNT/ZnO/NiO HNCs was evaluated by FESEM as shown in Fig. 2. Smooth surface of the CNTs can be elucidated from the Fig. 2a(i&ii) with an outer diameter of about 17–22 nm. Fig. 2a(iii) shows the surface chemical composition of CNTs where single carbon element is noticed without any other impurities. Nearly similar morphology was observed for CNT/ZnO core-shells which is indicating the unmitigated coating of thin layer of ZnO shell on CNTs core without disrupting their original structure (Fig. 2b(i&ii)). Chemical compositions of the samples are revealing the material as CNT/ZnO composite without any other elements (Fig. 2b(iii)). Perfect coating of thin ZnO layer enhances the energy density of the electrode owing to its battery type behavior and also improves the active surface area. Decorated like structures on CNT/ZnO core-shells are evidenced from the Fig. 2c(i&ii). Primarily, the material decorated on CNT/ZnO core-shells is assumed as NiO and further confirmed from the EDS

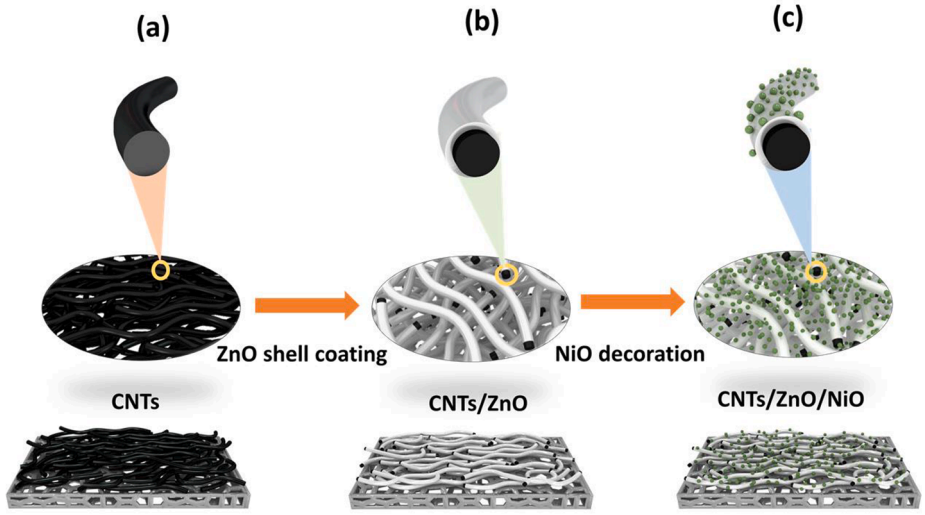

Fig. 1. Schematic representation of CNTs (a), CNT/ZnO core-shell nanostructures (b), and CNT/ZnO/NiO HNCs (c).

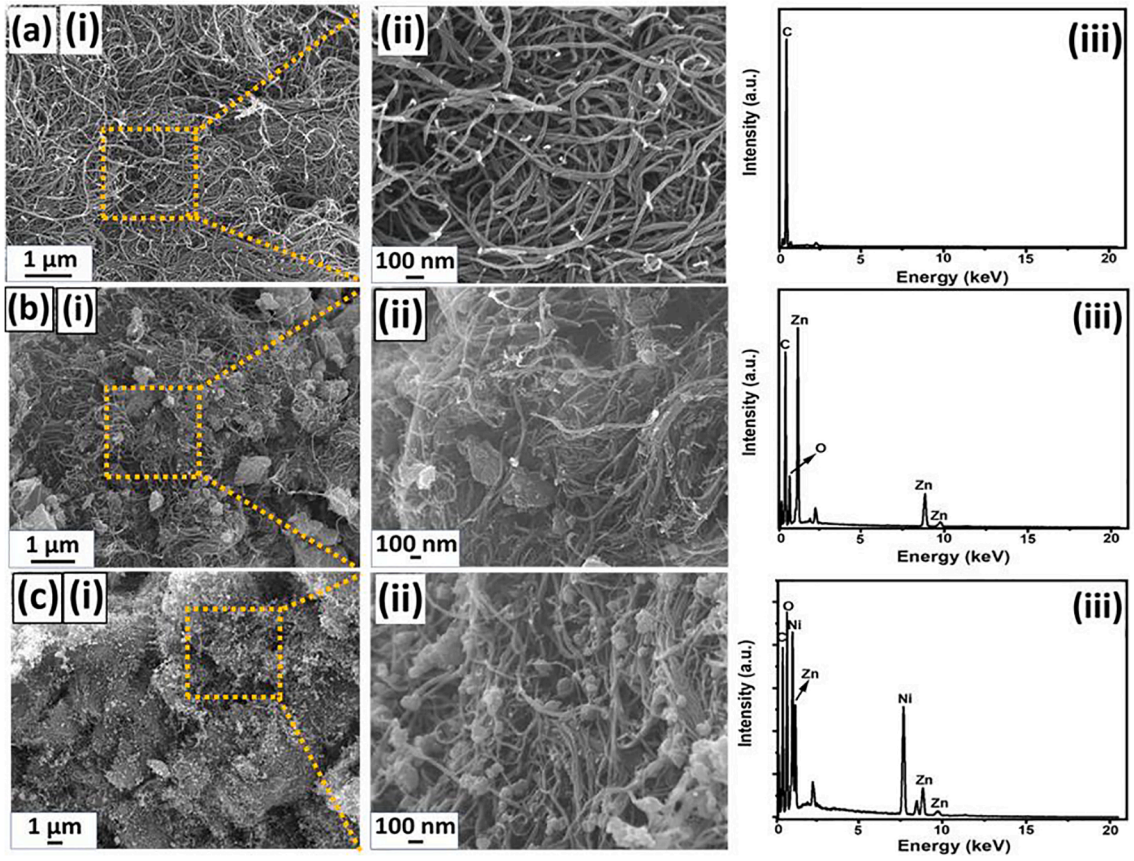

Fig. 2. Surface FESEM images and EDS spectra of CNTs (a)(i-iii), CNT/ZnO core-shell nanostructures (b)(i-iii), CNT/ZnO/NiO HNCs (c)(i-iii).

spectrum in Fig. 2c(iii), which shows that the material is composed of CNTs, ZnO, and NiO nanostructures. NiO decoration on CSNSs predominantly increases the electrochemical performance of the electrode with the aid of enhanced active surface area and excellent electrochemical properties of NiO [32]. Decorated structures improve the electrolyte diffusion into the core areas of the electrode and facilitate them to contribute to the overall electrode performance.

Fig. 3 gives the internal microstructural information of the CNT/ZnO/NiO HNCs. As can be seen from the Fig. 3a and 3b, decorated like nanostructures are clearly visible on the surface of CNTs. Further, to confirm the materials in the composite, lattice fringes were recorded at the points shown in yellow, red, and blue colors in Fig. 3a(i). Core-shell like structure is clearly revealed from the Fig. 3a(ii) in which CNT is a core and ZnO is a shell. The explicit view of ZnO shell and CNTs core is given in Fig. 3a(iii), where the d-spacing of 0.25 nm is attributed to the (002) plane of ZnO and the d-spacing of 0.35 nm is ascribed to the (002) plane of CNTs. Fig. 3a(iv) shows the lattice fringes of the CNT, ZnO, and NiO in the sample. The d-spacings of 0.35 nm, 0.285 nm, and 0.194 nm are assigned to the planes of CNTs (002), ZnO (100), and NiO (200), respectively and confirmed the decorated material as NiO. SAED patterns were utilized to substantiate the existence of the CNTs, ZnO, and NiO in the sample and observed the (002), (002), and (200) planes corresponding to the materials CNTs, ZnO, and NiO, respectively (Fig. 3c). Additionally, EDS elemental mapping was used for further investigation of the elemental composition in the sample and it lucidly reveals the presence of the elements like carbon, Zn, nickel, and oxygen in the sample (Fig. 3d(i-iv)).

Fig. 4 depicts the XRD patterns of CNTs, CNT/ZnO CSNSs, and CNT/ZnO/NiO HNCs, and XPS spectra of the CNT/ZnO/NiO HNCs sample. As shown in Fig. 4a, XRD patterns are demonstrating a most prominent peak located at 2Θ value of 26.1°, which is due to the graphitic structure plane (002) of pure CNTs. From the XRD patterns of CNT/ZnO, all the diffraction peaks other than CNTs (002) observed at 2Θ values of 31.7, 34.4, 36.2, 47.6, 56.6, 62.8, 67.9, and 69° are assigned to the planes of (100), (002), (101), (102), (110), (103), (112), and (201), respectively. All these observed planes are attributed to the hexagonal wurtzite structured ZnO in CNT/ZnO composite (JCPDC #89-1397). Furthermore, there are no other peaks noticed in the XRD patterns which is suggesting the perfect crystalline phase of the ZnO without any impurity elements. The XRD patterns of CNT/ZnO/NiO HNCs are showing the diffraction peaks related to NiO along with the peaks of CNTs and ZnO at 2Θ values of 43.4, 62.4, and 75.3° correspond to the planes (200), (220), and (311), respectively. All these planes are assigned to the cubic structured NiO (JCPDS #47-1049). Moreover, the XRD patterns of all the materials revealed the perfect phase and high purity of the prepared materials without any other impurity peaks. XPS survey spectrum of the CNT/ZnO/NiO HNCs displayed the signals related to the elements Zn, Ni, O, and C indicating their presence in the sample (Fig. 4b) and is well in agreement with the EDS results. Further, the high resolution XPS spectra were recorded for Zn 2p, Ni 2p, O 1s, and C 1s to verify their valence states in the composite. As shown in Fig. 4c, the high resolution XPS spectrum of Zn 2p is displaying the spin–orbit splitted Zn $2p_{3/2}$ and Zn $2p_{1/2}$ signals located at 1019.8 and 1042.9 eV, respectively. These are the characteristic peaks of divalent Zn (Zn^{2+}) [33]. Spin orbit splitting was also noticed in Ni 2p which is splitted into Ni $2p_{3/2}$ and Ni $2p_{1/2}$ with the peaks located at 854.1 and 871.6 eV, respectively (Fig. 4d). Small broad peaks presented at 859.88 and 877.78 eV in the spectrum are assigned to the satellite peaks of Ni $2p_{3/2}$ and Ni $2p_{1/2}$, respectively. All these main and satellite peaks are collectively indicating the Ni^{2+} state of the element Ni in the hybrid nanocomposite [34]. The major peak of C 1s core-level spectrum at 283 eV is deconvoluted into 3 peaks corresponding to C—C, C—OH, and C═O bonds, at 283, 283.7, and 287.6 eV, respectively (Fig. 4e) [35]. Fig. 4f divulges the narrow scan result of O 1s which is again deconvoluted into two peaks.

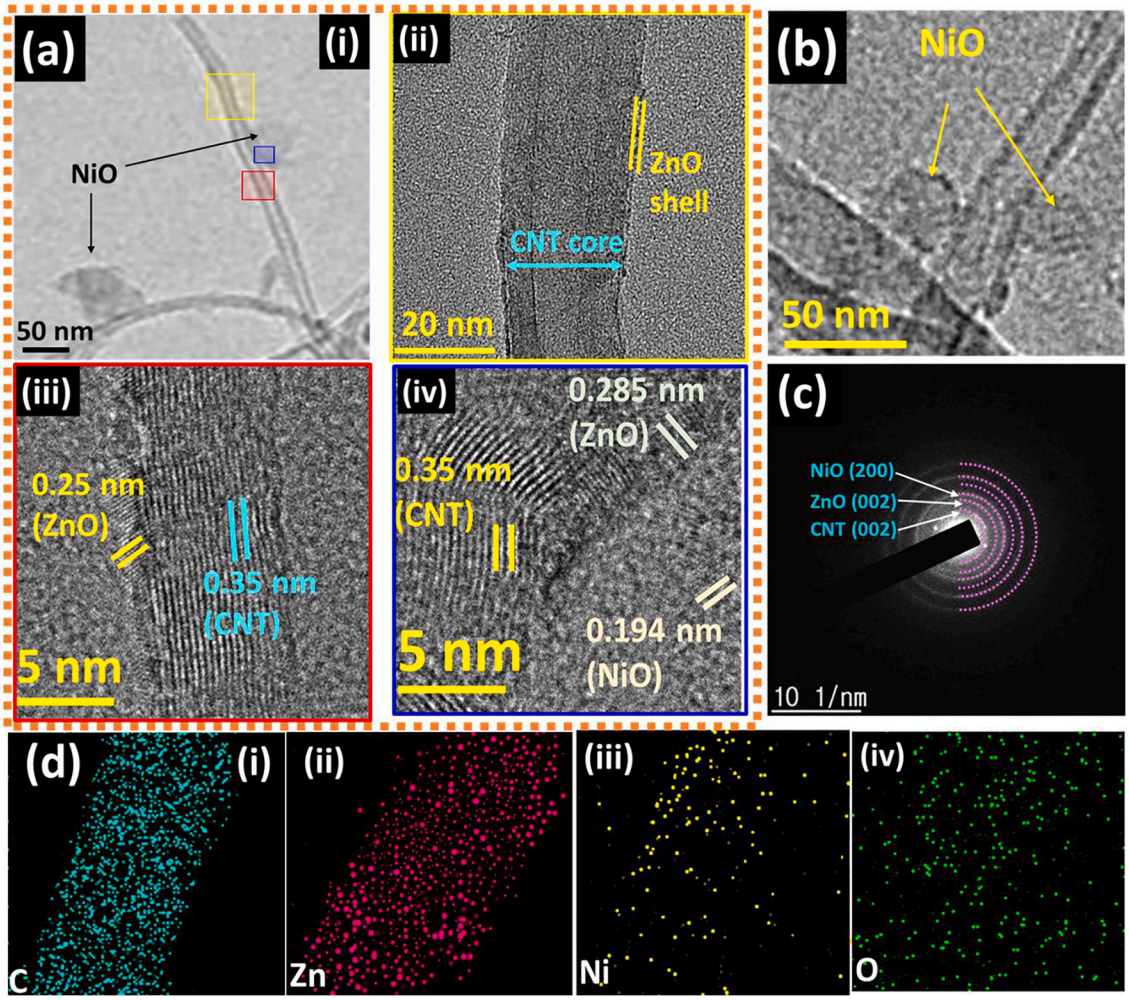

Fig. 3. HRTEM images of CNT/ZnO/NiO HNCs with different magnifications (a & b). SAED patterns of CNT/ZnO/NiO HNCs (c), elemental mapping of C, Zn, Ni, and O elements (d).

The peaks at 531.1 eV and 529.8 eV are the characteristic peaks of the OH^- and metal-oxygen bonding, respectively [8]. All these characterizations of the samples declared that the facilely fabricated materials achieved the good crystallinity and phase purity without any unwanted impurities.

3.2. Electrochemical performance of the electrodes

Fig. 5a manifests the CV curves of all the electrodes in three-electrode configuration recorded within the voltage range of 0–0.55 V at a constant sweep rate of 50 mV s^{-1} for comparison. From the figure it is evident that all the electrodes exemplified dominant redox peaks during forward as well as backward scans which is realized as the Faradaic mechanism of charge storage. Specifically, the area enclosed by the CV curve of CNT/ZnO/NiO HNCs/NF electrode is larger and the intensity of the redox peaks is also higher compared to other electrodes which is mainly due to the synergistic effect emerged from the combination of three different materials. Moreover, the decorated like structure of NiO on CNT/ZnO core-shell surface improved the electro-active sites and facilitated the large number of electrolyte ions to diffuse into the core levels of the electrode and contributed to the overall capacity. Charge/discharge characteristics of all the electrodes were examined using GCD curves at a steady current density of 5 mA cm^{-2} as shown in Fig. 5b. As can be perceived from the figure, the discharging time of the CNT/ZnO/NiO HNCs/NF electrode is longer than the other electrodes. This longer discharging time is attributed to the typical morphology of CNT/ZnO/NiO HNCs/NF with improved surface area. The decoration of NiO on CNT/ZnO core-shell nanostructures aided to perform the numerous reversible redox reactions as well as to store abundant charges. Areal capacity values of all the electrodes were calculated using the Eq. (1) and graphically shown in Fig. 5c. As expected, the CNT/ZnO/NiO HNCs/NF electrode has delivered highest areal capacity due to its larger discharge time. Owing to these results, CNT/ZnO/NiO HNCs/NF electrode was marked as optimized and studied its electrochemical behavior in detail. Fig. 5d presents the CV curves of the CNT/ZnO/NiO HNCs/NF electrode investigated at scan rates from 5 to 100 mV s^{-1}. As observed from the figure, all the CV curves contained redox peaks which is the characteristic behavior of battery type electrodes. Furthermore, the enclosed area of the CV curves and the value of the current were increased with scan rate and the electrode still holds its characteristic redox peaks even at high scan rates, stipulating the good reversibility of hybrid nanocomposite electrode.

Capacitive and diffusive controlled capacitance contribution was investigated by using the following power law.

$$i = av^b \tag{5}$$

where i is the peak current (mA), v is the scan rate (mV/s), a and b are the adjustable parameters. The value of b indicates the charge storage mechanism of the electrode. If the estimated value of b is close to 1, then the mechanism is capacitive controlled and if it is close to 0.5, the mechanism is battery type in which ionic diffusion takes place.

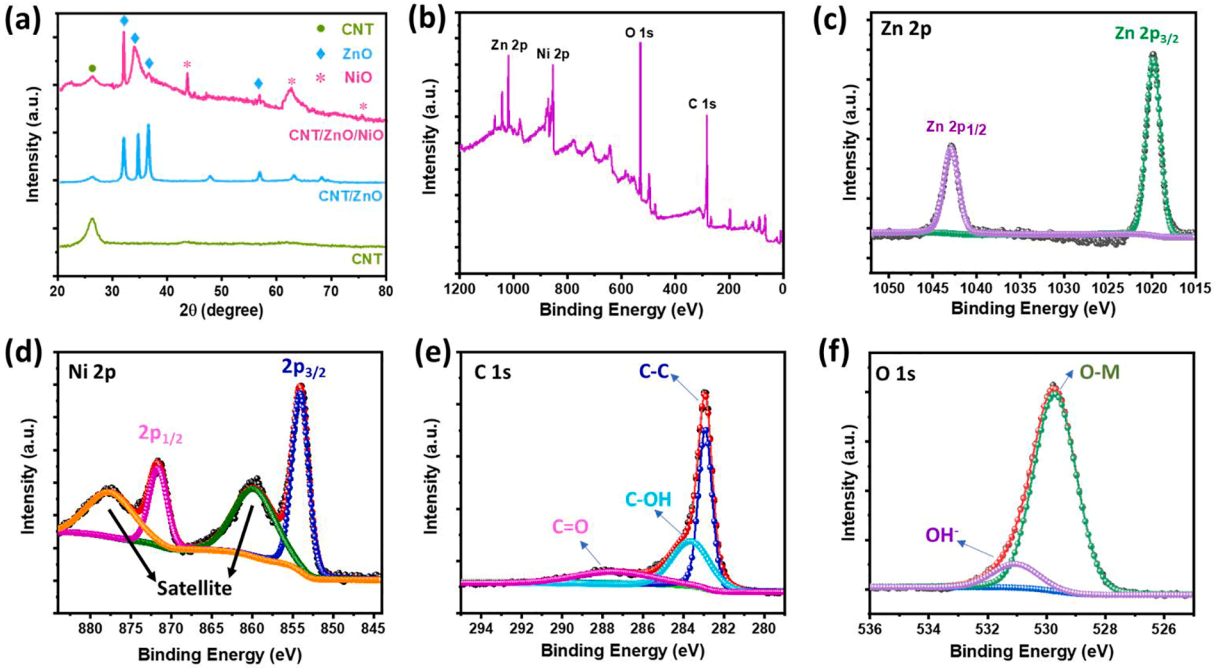

Fig. 4. XRD patterns of CNTs, CNT/ZnO, and CNT/ZnO/NiO HNCs (a). XPS survey spectrum of CNT/ZnO/NiO HNCs (b). Core-level spectra of elements Zn (c), Ni (d), C (e), and O (f) in the sample.

Generally, the value of b can be estimated from the slope of the graph between log(peak current) and log(scan rate). As can be seen from the Fig. 5e, the values of b for anodic and cathodic graphs are 0.58 and 0.67, respectively, corroborating the combination of capacitive and battery type charge storage behaviors of CNT/ZnO/NiO HNCs/NF electrode. Further, the power was converted as follows to calculate the contributions of each type [8]:

$$i = k_1 v + k_2 v^{1/2} \tag{6}$$

where, k_1, and k_2 are the parameters, whose values can be realized from the slope and intercept of the linear curves in Fig. 5f. Fig. 5g shows the percentages of capacitive and diffusive controlled current contributions. At the low scan rates, the current contribution is mainly diffusion controlled, which is gradually decreased with scan rate. Diffusion controlled current contribution is nearly 94% at a scan rate of 5 mV s^{-1} and 78% at a scan rate of 100 mV s^{-1}, indicating the domination of battery-type behavior at all scan rates. Capacitive controlled current contribution is increased from 6% to 22% with the increase in scan rates from 5 mV s^{-1} to 100 mV s^{-1}.

GCD cycles were also recorded for CNT/ZnO/NiO HNCs/NF electrode at various current densities ranging from 3 mA cm^{-2} to 20 mA cm^{-2} and the obtained results are shown in Fig. 5h. As noticed from the figure, the GCD cycles of hybrid nanocomposite electrode are well in accordance with CV curves, corroborating its battery type charge storage mechanism. The values of areal capacity were calculated at each of the current density and shown in Fig. 5i. Hybrid nanocomposite electrode has shown high areal capacities of 66.7, 41.4, 35.8, 36.7, 34, 28.3, and 21.1 μAh cm^{-2} at current densities of 3, 5, 7, 10, 12, 15, and 20 mA cm^{-2}, respectively. As we know, it is very essential for any electrode material to hold good stability and repeatability during various charge/discharge operations in order to satisfy the demand of practical applications. Thus, CNT/ZnO/NiO HNCs/NF electrode was subjected to cycling stability test by observing the charge/discharge cycles without break until 3000 cycles at a constant current density of 5 mA cm^{-2}. As can be observed from the Fig. 5j, the electrode has shown good stability during the test with an exceptional capacity retention of 112% at the end of 3000th cycle. The enhancement in the capacity retention after first few cycles is ascribed to the activation of CNT/ZnO/NiO HNCs electrode material in electrolyte and improvement in the discharge time as shown in the inset of the figure. Electrochemical impedance spectroscopy was adopted to analyze equivalent series resistance of the hybrid nanocomposite electrodes before and after the cycling stability test as presented in Fig. 5k. Nyquist plots were recorded in the frequency range from 0.1 to 100 kHz with an open-circuit voltage of 5 mV. Nyquist plots corresponding to before test and after test were fitted by applying an equivalent circuit as shown in the inset of the Fig. 5h using Zview software. The Nyquist plot's intercepting point on X-axis gives the information about internal resistance of the device (R1) which is the combination of active material internal resistance, electrolyte resistance, and contact resistance between current collector and active electrode material. Charge transfer resistance (R2) can be estimated from the diameter of the semicircle appeared at high-middle frequency region. The observed R1 and R2 values from the fitted EIS curves of the electrode before cycling test were 0.192 Ω and 0.22 Ω, respectively. While, the R1 and R2 values of the electrode after cycling test were 0.486 Ω and 0.63 Ω, respectively, indicating a slight increase in the values after long-term operations. The low values of R1 and R2 were due to the conductive CNTs and special structure of the hybrid nanocomposites. A schematical representation of the CNT/ZnO/NiO HNCs/NF electrode including its morphological features is given in Fig. 5l. The decorated like structure of NiO allows the electrolyte to diffuse into the core levels of the electrode efficaciously and promotes their participation in the electrochemical reactions. Moreover, conductive CNTs facilitated the quick transport of electrons (obtained during the charging and discharging processes) from the active material to the current collector (NF). Owing to these features, the CNT/ZnO/NiO HNCs/NF electrode has shown high areal capacities with good stability and reversibility than other electrodes.

A hybrid supercapacitor was fabricated using CNT/ZnO/NiO/NF as a positive electrode, and CNT/NF as a negative electrode. Cellulose filter paper and 1 M KOH were used as separator and electrolyte, respectively. Electrochemical properties of CNT/NF were studied and presented in Fig. S2 of ESI with appropriate analyses. Prior to the HSC fabrication, both electrodes as well as separator were soaked in electrolyte and then cautiously assembled into a device as schematically shown in Fig. 6a. It

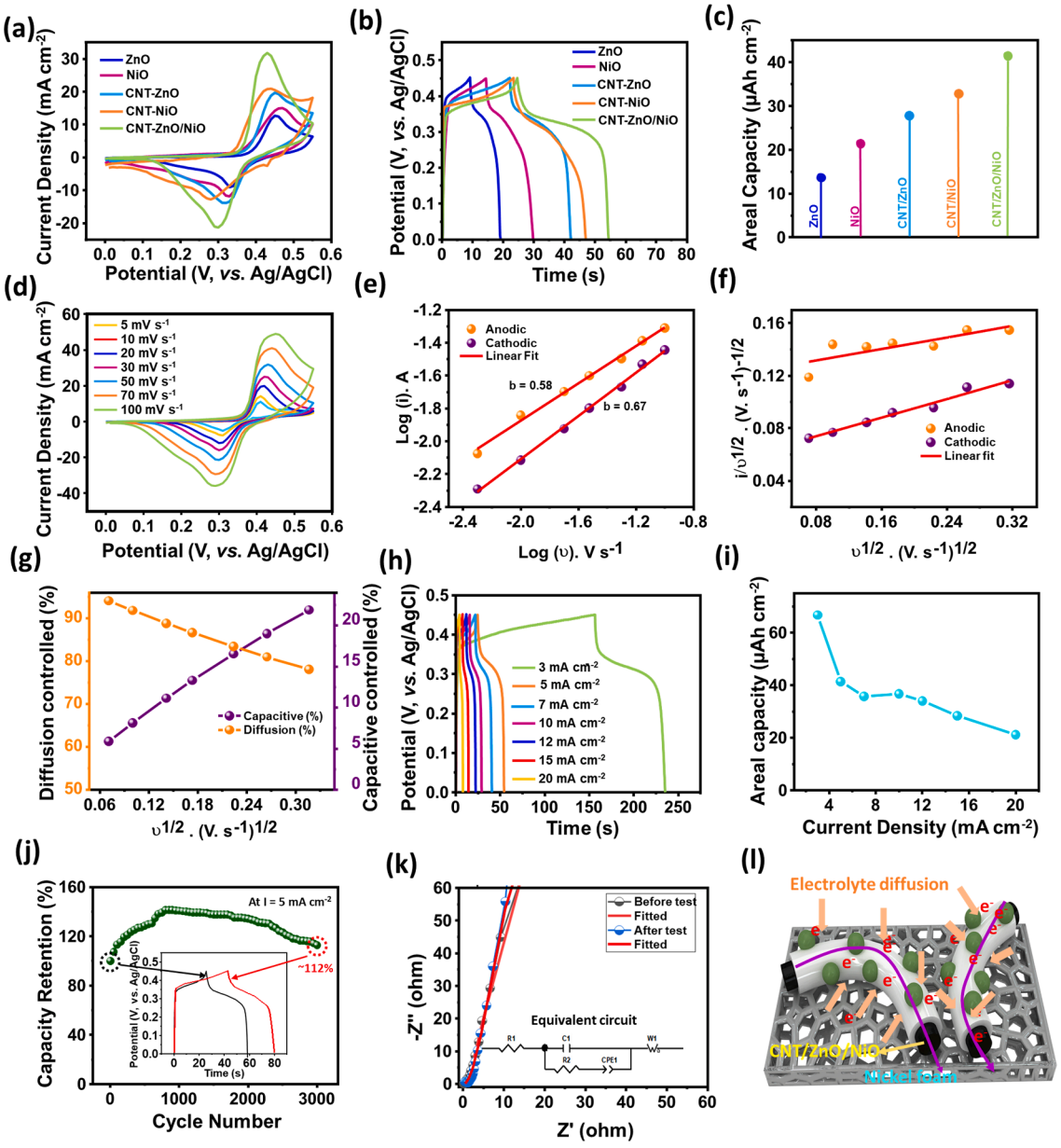

Fig. 5. Comparative CV (a), GCD (b) curves, and calculated areal capacities (c) of all the materials. CV curves of CNT/ZnO/NiO HNCs/NF electrode recorded at various scan rates (d). Relationship between Log (i) and Log (υ) (e), and $i/\upsilon^{1/2}$ $\upsilon^{1/2}$ (f). Capacitive and diffusive current contributions of CNT/ZnO/NiO HNCs/NF electrode (g). GCD curves of CNT/ZnO/NiO HNCs/NF at different current densities (h). Areal capacity values of CNT/ZnO/NiO HNCs/NF electrode at different current densities (i). Cycling stability (j) and EIS curves (k) of CNT/ZnO/NiO HNCs/NF electrode. Schematic diagram illustrating the CNT/ZnO/NiO HNCs/NF electrode (l).

is recommended to balance the masses of the active materials before constructing a supercapacitor to achieve high performance. Hence, optimization of the mass was done using the following equation after several experiments [36].

$$m_{-} = \frac{Q_{+} \times a_{+}}{C_{-} \times \Delta V_{-}} \tag{7}$$

where, m_{-}, C_{-}, and ΔV_{-} are the mass, areal capacity, and potential window of the negative electrode, respectively. Q_{+} and a_{+} are the areal capacity and active area of the positive electrode, respectively. The optimized mass of the negative electrode from the above equation was about ~1.2 mg. The potential window of the fabricated supercapacitor was optimized by analyzing the CV curves at diverse potential windows ranging from 0 to 0.6 V to 0–1.4 V as shown in Fig. 6b & S3. As can be perceived from the figure, all the CV curves retained their original shape without any deformation until 0–1.3 V and showed a sharp peak for the potential window 0–1.4 V (due to the oxygen/hydrogen evolution), indicating the 0–1.3 V as the best suitable potential window. Further, GCD curves of the device were recorded by varying the voltage range from 0.5 to 1.3 V at a constant current density of 12 mA cm^{-2} (Fig. 6c). From the figure, clear triangular shapes were observed at lower potentials where the capacitive mechanism is dominant and with an increase in the potential range, the shape is slightly changed indicating the presence of capacitive and battery type mechanisms. From the CV and GCD curves which were recorded at different potentials, 1.3 V was considered as optimum potential and performed detailed electrochemical analysis of the fabricated device at this potential. Fig. 6d presents the CV curves of the HSC device at different scan rates ranging from 10 to 100 mV s^{-1}. Due to the combination of battery type and electric double layer type materials in the device, the obtained CV curves

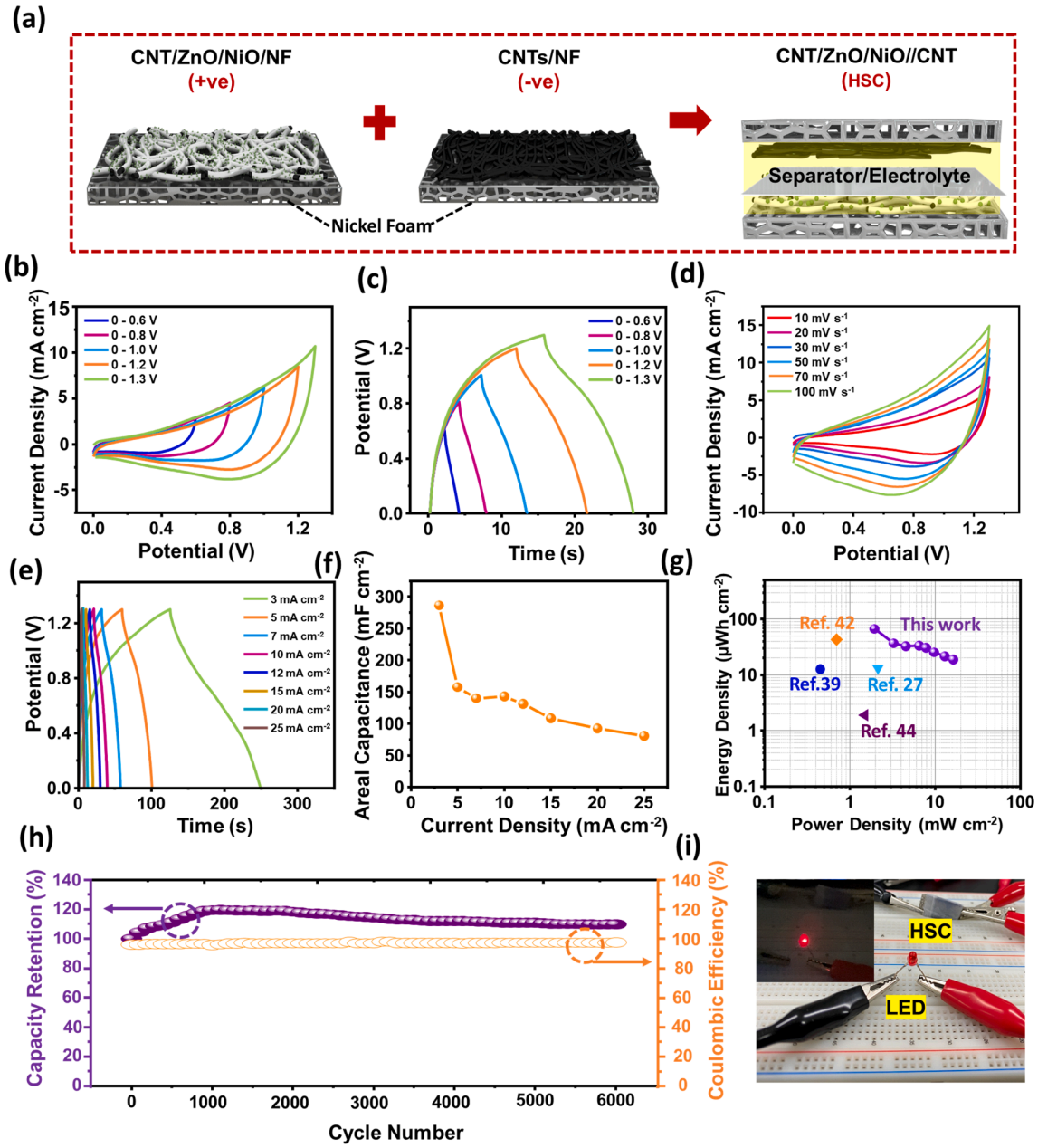

Fig. 6. Schematic illustration of the HSC device with CNT/ZnO/NiO/NF positive electrode and CNTs/NF negative electrode (a). CV (b), and GCD (c) curves of the HSC device with varying potential ranges. CV (d), and GCD (e) curves of HSC device at various scan rates, and current densities, respectively. Areal capacitances of the HSC device at different current densities (f). Ragone plot showing the energy and power densities of HSC device (g). Cycling stability of the HSC device studied up to 6000 cycles (h). Illustration of HSC device viability by powering up LED (i).

are showing quasi-rectangle shapes. Further, GCD measurements were carried out to examine the electrochemical performance of the device at fixed potential range of 0–1.3 V by varying the current densities from 3 to 25 mA cm^{-2} (Fig. 6e). The areal capacitance values were calculated using Eq. (2) corresponding to each of the applied current densities from GCD curves and graphically represented in Fig. 6f. The calculated areal capacitances of the device are 286.6, 157.7, 140, 143.1, 131.1, 108.5, 92.3, and 80.8 mF cm^{-2} corresponding to the current densities of 3, 5, 7, 10, 12, 15, 20, and 25 mA cm^{-2}, respectively. Further, areal energy density and power density of the device were calculated using Eq. (3&4) and presented in Fig. 6g. The device exhibited high areal energy density of 67 μWh cm^{-2} at a power density of 1.95 mW cm^{-2}. Further, the device shown good performance under high current density of 25 mA cm^{-2} with an areal energy density of ~20 μWh cm^{-2} at a high power density of 16.25 mW cm^{-2}. The obtained areal energy density and power density values of the present supercapacitor are larger than the values of recently reported CNT based SCs [27,37–45]. As the cycling stability is particularly important to employ the device in practical applications, the cycling test was conducted for 6000 cycles. As can be seen from the Fig. 6h, the HSC device has retained its areal capacitance nearly 109% after 6000 cycles. This good stability in the capacitance is attributed to the synergistic effect originated from the three different materials in positive electrode and highly stable CNTs based negative electrode. Finally, making the use of high energy density and power density of the device, it has been tested for its feasibility by illuminating commercial LED. As can be elucidated from the Fig. 6i, the device was successfully illuminated the LED after charging for a while. Table S1 shows the comparison of the energy and power densities of previously reported CNT based supercapacitors with present CNT/ZnO/NiO//CNT supercapacitor. From the morphological advantages, high areal capacitances,

and high energy and power densities, the fabricated HSC device is expected to employ in energy storage applications successfully.

4. Conclusions

In summary, NiO decorated CNT/ZnO core-shell hybrid nanocomposites were facilely prepared by a two-step solution-based technique. Uniform distribution of thin ZnO layer on CNTs surface and NiO decoration on CNT/ZnO surface were elucidated from the morphology investigations. Structural and compositional studies revealed the perfect crystalline phase of the materials without any impurities. All the prepared materials were used to fabricate electrodes by simple slurry coating method on NF. CNT/ZnO/NiO HNCs/NF electrode has shown high areal capacity of ~67 μAh cm^{-2} at a current density of 3 mA cm^{-2} with a cycling stability of 112% upto 3000 cycles. NiO decoration on CNT/ZnO surface ultimately improved the electro-active area thereby effective electrolyte ions diffusion which helped in performance augmentation. Collective advantages of CNTs, ZnO, and NiO are contributed to the enhanced electrochemical properties of CNT/ZnO/NiO HNCs/NF electrode. HSC device was fabricated with CNT/ZnO/NiO HNCs/NF and CNT/NF as positive and negative electrodes, respectively. The fabricated HSC device demonstrated high areal energy density of 67 μWh cm^{-2} and power density of 16.25 mW cm^{-2} at current densities of 3 mA cm^{-2} and 25 mA cm^{-2}, respectively. Moreover, the device has shown outstanding stability over 6000 cycles with ~109% of capacity retention. Ultimately, the technology of decorating NiO on CNTs and metal oxide core-shell surfaces shows promising impacts on the enhancement of the electrochemical performance.

CRediT authorship contribution statement

Nagabandi Jayababu: Conceptualization, Methodology, Data curation, Investigation, Formal analysis, Validation, Visualization, Writing - original draft. **Seungju Jo:** Data curation. **Youngsu Kim:** Data curation. **Daewon Kim:** Data curation, Validation, Funding acquisition, Project administration, Supervision.

Declaration of Competing Interest

The authors declare that they have no known competing financial interests or personal relationships that could have appeared to influence the work reported in this paper.

Acknowledgements

This research was supported by the Basic Science Research Program through the National Research Foundation of Korea (NRF) funded by the Ministry of Education (2018R1A6A1A03025708). This work was also supported by a grant from the National Research Foundation of Korea (NRF) funded by the Korean government (MSIT) (No. NRF-2018R1C1B5045747).

Appendix A. Supplementary data

Supplementary data to this article can be found online at https://doi.org/10.1016/j.ultsonch.2020.105374.

References

[1] L. Zhang, D. Shi, T. Liu, M. Jaroniec, J. Yu, Nickel-based materials for supercapacitors, Mater. Today 25 (2019) 35–65, https://doi.org/10.1016/j.mattod.2018.11.002.
[2] A. González, E. Goikolea, J.A. Barrena, R. Mysyk, Review on supercapacitors: technologies and materials, Renew. Sustain. Energy Rev. 58 (2016) 1189–1206, https://doi.org/10.1016/j.rser.2015.12.249.
[3] Y. Shao, M.F. El-Kady, J. Sun, Y. Li, Q. Zhang, M. Zhu, H. Wang, B. Dunn, R. B. Kaner, Design and mechanisms of asymmetric supercapacitors, Chem. Rev. 118 (18) (2018) 9233–9280, https://doi.org/10.1021/acs.chemrev.8b00252.
[4] S. Mekhilef, R. Saidur, A. Safari, A review on solar energy use in industries, Renew. Sustain. Energy Rev. 15 (4) (2011) 1777–1790, https://doi.org/10.1016/j.rser.2010.12.018.
[5] D.Y.C. Leung, Y. Yang, Wind energy development and its environmental impact: a review, Renew. Sustain. Energy Rev. 16 (1) (2012) 1031–1039, https://doi.org/10.1016/j.rser.2011.09.024.
[6] N. Khan, A. Kalair, N. Abas, A. Haider, Review of ocean tidal, wave and thermal energy technologies, Renew. Sustain. Energy Rev. 72 (2017) 590–604, https://doi.org/10.1016/j.rser.2017.01.079.
[7] I. Ullah Khan, M. Hafiz Dzarfan Othman, H. Hashim, T. Matsuura, A.F. Ismail, M. Rezaei-DashtArzhandi, I. Wan Azelee, Biogas as a renewable energy fuel – a review of biogas upgrading, utilisation and storage, Energy Convers. Manage. 150 (2017) 277–294, https://doi.org/10.1016/j.enconman.2017.08.035.
[8] B. Ramulu, G. Nagaraju, S. Chandra Sekhar, S.K. Hussain, D. Narsimulu, J.S. Yu, Synergistic effects of cobalt molybdate@phosphate core–shell architectures with ultrahigh capacity for rechargeable hybrid supercapacitors, ACS Appl. Mater. Interfaces 11 (44) (2019) 41245–41257, https://doi.org/10.1021/acsami.9b11707.
[9] S. Kumar, G. Saeed, N.H. Kim, J.H. Lee, Fabrication of Co–Ni–Zn ternary Oxide@NiWO4 core-shell nanowire arrays and Fe2O3-CNTs@GF for ultra-high-performance asymmetric supercapacitor, Compos. B Eng. 176 (2019) 107223, https://doi.org/10.1016/j.compositesb:2019.107223.
[10] F. Wang, X. Wu, X. Yuan, Z. Liu, Y.i. Zhang, L. Fu, Y. Zhu, Q. Zhou, Y. Wu, W. Huang, Latest advances in supercapacitors: from new electrode materials to novel device designs, Chem. Soc. Rev. 46 (22) (2017) 6816–6854, https://doi.org/10.1039/c7cs00205j.
[11] Q. Zhu, D. Zhao, M. Cheng, J. Zhou, K.A. Owusu, L. Mai, Y. Yu, A new view of supercapacitors: integrated supercapacitors, Adv. Energy Mater. 9 (36) (2019) 1901081, https://doi.org/10.1002/aenm.201901081.
[12] Y.u. Zhang, H. Hu, Z. Wang, B. Luo, W. Xing, L.i. Li, Z. Yan, L. Wang, Boosting the performance of hybrid supercapacitors through redox electrolyte-mediated capacity balancing, Nano Energy 68 (2020) 104226, https://doi.org/10.1016/j.nanoen.2019.104226.
[13] T. Brousse, D. Bélanger, J.W. Long, To be or not to be pseudocapacitive? J. Electrochem. Soc. 162 (5) (2015) A5185–A5189, https://doi.org/10.1149/2.0201505jes.
[14] G. Sun, Y. Xiao, B. Lu, X. Jin, H. Yang, C. Dai, X. Zhang, Y. Zhao, L. Qu, Hybrid energy storage device: combination of zinc-ion supercapacitor and zinc–air battery in mild electrolyte, ACS Appl. Mater. Interfaces 12 (6) (2020) 7239–7248, https://doi.org/10.1021/acsami.9b20629.
[15] L. Kebabsa, J. Kim, D. Lee, B. Lee, Highly porous cobalt oxide-decorated carbon nanofibers fabricated from starch as free-standing electrodes for supercapacitors, Appl. Surf. Sci. 511 (2020) 145313, https://doi.org/10.1016/j.apsusc.2020.145313.
[16] X. Liu, G. Sheng, M. Zhong, X. Zhou, Hybrid nanowires and nanoparticles of WO 3 in a carbon aerogel for supercapacitor applications, Nanoscale 10 (9) (2018) 4209–4217, https://doi.org/10.1039/c7nr07191d.
[17] C. Xiang, Y. Liu, Y. Yin, P. Huang, Y. Zou, M. Fehse, Z. She, F. Xu, D. Banerjee, D. Hermida Merino, A. Longo, H.-B. Kraatz, D.F. Brougham, B. Wu, L. Sun, Facile green route to Ni/Co oxide nanoparticle embedded 3D graphitic carbon nanosheets for high performance hybrid supercapacitor devices, ACS Appl. Energy Mater. 2 (5) (2019) 3389–3399.
[18] S.K. Kandasamy, K. Kandasamy, Recent advances in electrochemical performances of graphene composite (graphene-polyaniline/polypyrrole/activated carbon/carbon nanotube) electrode materials for supercapacitor: a review, J. Inorg. Organomet. Polym. 28 (3) (2018) 559–584, https://doi.org/10.1007/s10904-018-0779-x.
[19] Z. Chen, V. Augustyn, J. Wen, Y. Zhang, M. Shen, B. Dunn, Y. Lu, High-performance supercapacitors based on intertwined CNT/V2O5 nanowire nanocomposites, Adv. Mater. 23 (6) (2011) 791–795, https://doi.org/10.1002/adma.201003658.
[20] C. Sasirekha, S. Arumugam, G. Muralidharan, Green synthesis of ZnO/carbon (ZnO/C) as an electrode material for symmetric supercapacitor devices, Appl. Surf. Sci. 449 (2018) 521–527, https://doi.org/10.1016/j.apsusc.2018.01.172.
[21] X. Xiao, B. Han, G. Chen, L. Wang, Y. Wang, Preparation and electrochemical performances of carbon sphere@ZnO core-shell nanocomposites for supercapacitor applications, Sci. Rep. 7 (1) (2017), https://doi.org/10.1038/srep40167.
[22] X. Zheng, X. Yan, Y. Sun, Z. Bai, G. Zhang, Y. Shen, Q. Liang, Y. Zhang, Au-embedded ZnO/NiO hybrid with excellent electrochemical performance as advanced electrode materials for supercapacitor, ACS Appl. Mater. Interfaces 7 (4) (2015) 2480–2485, https://doi.org/10.1021/am5073468.
[23] R. Ranjithkumar, S.E. Arasi, S. Sudhahar, N. Nallamuthu, P. Devendran, P. Lakshmanan, M.K. Kumar, Enhanced electrochemical studies of ZnO/CNT nanocomposite for supercapacitor devices, Physica B 568 (2019) 51–59, https://doi.org/10.1016/j.physb.2019.05.025.
[24] W. Wang, S. Jiao, J. Cao, H.E. Naguib, Zinc oxide/carbon nanotube nanocomposite for high-performance flexible supercapacitor with sensing ability, Electrochim. Acta 350 (2020) 136353, https://doi.org/10.1016/j.electacta.2020.136353.
[25] N.I.T. Ramli, S.A. Rashid, M.S. Mamat, Y. Sulaiman, S.A. Zobir, S. Krishnan, Incorporation of zinc oxide into carbon nanotube/graphite nanofiber as high performance supercapacitor electrode, Electrochim. Acta 228 (2017) 259–267, https://doi.org/10.1016/j.electacta.2017.01.068.
[26] Y. Zhang, B. Lin, J. Wang, J. Tian, Y. Sun, X. Zhang, H. Yang, All-solid-state asymmetric supercapacitors based on ZnO quantum dots/carbon/CNT and porous N-doped carbon/CNT electrodes derived from a single ZIF-8/CNT template,

J. Mater. Chem. A 4 (26) (2016) 10282–10293, https://doi.org/10.1039/c6ta03633c.
[27] Y. Li, X. Yan, X. Zheng, H. Si, M. Li, Y. Liu, Y. Sun, Y. Jiang, Y. Zhang, Fiber-shaped asymmetric supercapacitors with ultrahigh energy density for flexible/wearable energy storage, J. Mater. Chem. A 4 (45) (2016) 17704–17710, https://doi.org/10.1039/C6TA07163E.
[28] E. Samuel, T.-G. Kim, C.-W. Park, B. Joshi, M.T. Swihart, S.S. Yoon, Supersonically sprayed Zn2SnO4/SnO2/CNT nanocomposites for high-performance supercapacitor electrodes, ACS Sustainable Chem. Eng. 7 (16) (2019) 14031–14040, https://doi.org/10.1021/acssuschemeng.9b02549.
[29] Y. Li, Q. Wei, R. Wang, J. Zhao, Z. Quan, T. Zhan, D. Li, J. Xu, H. Teng, W. Hou, 3D hierarchical porous nitrogen-doped carbon/Ni@NiO nanocomposites self-templated by cross-linked polyacrylamide gel for high performance supercapacitor electrode, J. Colloid Interface Sci. 570 (2020) 286–299, https://doi.org/10.1016/j.jcis.2020.03.004.
[30] F. Liu, X. Wang, J. Hao, S. Han, J. Lian, Q. Jiang, High density arrayed Ni/NiO core-shell nanospheres evenly distributed on graphene for ultrahigh performance supercapacitor, Sci. Rep. 7 (1) (2017), https://doi.org/10.1038/s41598-017-17899-6.
[31] S.C. Sekhar, G. Nagaraju, J.S. Yu, Conductive silver nanowires-fenced carbon cloth fibers-supported layered double hydroxide nanosheets as a flexible and binder-free electrode for high-performance asymmetric supercapacitors, Nano Energy 36 (2017) 58–67, https://doi.org/10.1016/j.nanoen.2017.04.019.
[32] J. Cheng, B. Zhao, W. Zhang, F. Shi, G. Zheng, D. Zhang, J. Yang, High-performance supercapacitor applications of NiO-nanoparticle-decorated millimeter-long vertically aligned carbon nanotube arrays via an effective supercritical CO2-assisted method, Adv. Funct. Mater. 25 (47) (2015) 7381–7391, https://doi.org/10.1002/adfm.201502711.
[33] N. Jayababu, M. Poloju, J. Shruthi, M.V.R. Reddy, Synthesis of ZnO/NiO nanocomposites for the rapid detection of ammonia at room temperature, Mater. Sci. Semicond. Process. 102 (2019) 104591, https://doi.org/10.1016/j.mssp.2019.104591.
[34] N. Jayababu, M. Poloju, J. Shruthi, M.V.R. Reddy, Semi shield driven p-n heterostructures and their role in enhancing the room temperature ethanol gas sensing performance of NiO/SnO2 nanocomposites, Ceram. Int. 45 (12) (2019) 15134–15142, https://doi.org/10.1016/j.ceramint.2019.04.255.
[35] C. Min, Z. He, H. Song, D. Liu, W. Jia, J. Qian, Y. Jin, L. Guo, Fabrication of novel CeO2/GO/CNTs ternary nanocomposites with enhanced tribological performance, Appl. Sci. (2019), https://doi.org/10.3390/app9010170.
[36] G.K. Veerasubramani, A. Chandrasekhar, M.S.P. Sudhakaran, Y.S. Mok, S.J. Kim, Liquid electrolyte mediated flexible pouch-type hybrid supercapacitor based on binderless core–shell nanostructures assembled with honeycomb-like porous carbon, J. Mater. Chem. A 5 (22) (2017) 11100–11113, https://doi.org/10.1039/c7ta01308f.
[37] H. Xu, X. Hu, H. Yang, Y. Sun, C. Hu, Y. Huang, Flexible asymmetric micro-supercapacitors based on Bi2O3 and MnO2 nanoflowers: larger areal mass promises higher energy density, Adv. Energy Mater. 5 (6) (2015) 1401882, https://doi.org/10.1002/aenm.201401882.
[38] S. Chandra Sekhar, G. Nagaraju, D. Narsimulu, B. Ramulu, S.K. Hussain, J.S. Yu, Graphene matrix sheathed metal vanadate porous nanospheres for enhanced longevity and high-rate energy storage devices, ACS Appl. Mater. Interfaces 12 (24) (2020) 27074–27086, https://doi.org/10.1021/acsami.0c04170.
[39] Z. Yang, Y.u. Yang, C.-X. Lu, Y.-y. Zhang, X.-H. Zhang, Y.-y. Liu, A high energy density fiber-shaped supercapacitor based on zinc-cobalt bimetallic oxide nanowire forests on carbon nanotube fibers, New Carbon Mater. 34 (6) (2019) 559–568, https://doi.org/10.1016/S1872-5805(19)60031-4.
[40] G. Huang, Y.e. Zhang, L. Wang, P. Sheng, H. Peng, Fiber-based MnO2/carbon nanotube/polyimide asymmetric supercapacitor, Carbon 125 (2017) 595–604, https://doi.org/10.1016/j.carbon.2017.09.103.
[41] X. Lu, Y. Bai, R. Wang, J. Sun, A high-performance flexible and weavable asymmetric fiber-shaped solid-state supercapacitor enhanced by surface modifications of carbon fibers with carbon nanotubes, J. Mater. Chem. A 4 (46) (2016) 18164–18173, https://doi.org/10.1039/c6ta08233e.
[42] C. Choi, J.W. Park, K.J. Kim, D.W. Lee, M.J. de Andrade, S.H. Kim, S. Gambhir, G. M. Spinks, R.H. Baughman, S.J. Kim, Weavable asymmetric carbon nanotube yarn supercapacitor for electronic textiles, RSC Adv. 8 (24) (2018) 13112–13120, https://doi.org/10.1039/c8ra01384e.
[43] P.K. Adusei, S.N. Kanakaraj, S. Gbordzoe, K. Johnson, D. DeArmond, Y.-Y. Hsieh, Y. Fang, S. Mishra, N. Phan, N.T. Alvarez, V. Shanov, A scalable nano-engineering method to synthesize 3D-graphene-carbon nanotube hybrid fibers for supercapacitor applications, Electrochim. Acta 312 (2019) 411–423, https://doi.org/10.1016/j.electacta.2019.04.179.
[44] W. Yang, L. He, X. Tian, M. Yan, H. Yuan, X. Liao, J. Meng, Z. Hao, L. Mai, Carbon-MEMS-based alternating stacked MoS2@rGO-CNT micro-supercapacitor with high capacitance and energy density, Small 13 (26) (2017) 1700639, https://doi.org/10.1002/smll.201700639.
[45] J.-A. Wang, C.-C. Ma, C.-C. Hu, Constructing a high-performance quasi-solid-state asymmetric supercapacitor: NaxMnO2@CNT/WPU-PAAK-Na2SO4/AC-CNT, Electrochim. Acta 334 (2020) 135576, https://doi.org/10.1016/j.electacta.2019.135576.